CrystEngComm

Accepted Manuscript

ROYAL SOCIETY OF CHEMISTRY

www.rsc.org/crystengcomm

CrystEngComm

Dynamic Article Links ►

Cite this: DOI: 10.1039/c5ce00000x

www.rsc.org/CrystEngComm

ARTICLE

Coligand Syntheses, Crystal Structures, Luminscence and Photocatalystic Properties of Five Coordination Polymers Based on Rigid Tetracarboxylic Acids and Imidazole Linkers

Liming Fan,[a,b] Weiliu Fan,[a] Bin Li,[b] Xian Zhao*[a] and Xiutang Zhang*[a,b]

Received (in XXX, XXX) Xth XXXXXXXXX 2015, Accepted Xth XXXXXXXXX 2015
DOI: 10.1039/c5ce00000x

ABSTRACT: Five coordination polymers (CPs) with distinct structures, namely, $[Cu(H_2tptc)(1,4\text{-bidb})]_n$ (**1**), $\{[Co_2(tptc)(1,3,5\text{-tib})(H_2O)]\cdot 7H_2O\}_n$ (**2**), $\{[Ni(tptc)_{0.5}(1,3\text{-bimb})]\cdot H_2O\}_n$ (**3**), $\{[Zn(qptc)_{0.5}(1,4\text{-bimb})]\cdot 3H_2O\}_n$ (**4**), and $\{[Zn(qptc)_{0.5}(1,3\text{-bimb})]\cdot H_2O\}_n$ (**5**) (H_4tptc = terphenyl-3,3",5,5"-tetracarboxylic acid, H_4qptc = quaterphenyl-3,3'",5,5'"-tetracarboxylic acid, 1,4-bidb = 1,4-bis(1-imidazol-yl)-2,5-dimethyl benzene, 1,3,5-tib = 1,3,5-tris(1-imidazol-yl)benzene, 1,3-bimb = 1,3-bis(imidazol-1-ylmethyl)benzene, 1,4-bimb= 1,4-bis(imidazol-1-ylmethyl)benzene), have been synthesized through the mixed ligands strategy. Complex **1** features a new 3D (4,6)–connected net with the Schläfli symbol of $(4^2\cdot 6^4)(4^2\cdot 6^8\cdot 7\cdot 8^4)$. Complex **2** displays a 3D 2-fold interpenetrated framework with the unprecedented (3,3,4,4)-connected $(6\cdot 8^2)_2(6^2\cdot 8^3\cdot 10)(6^2\cdot 8^4)$ topology. Complex **3** exhibits a $(3^2\cdot 6^2\cdot 7^2)$-**kgm** layer featured a 2D+2D→3D packing supramolecular structure interweaved through the [Ni(1,3-bimb)] lock knots. Complex **4** shows an unprecedented 3D (4,4)–connected 8^6 net. And complex **5** is also a 2D+2D→3D supramolecular structure featured by the **kgm** sheets hinged together through the [Zn(1,3-bimb)] lock knots. Besides, the luminescent properties of **4** and **5** have been investigated. Moreover, complexes **1-3** show relatively good photocatalytic activities for dye methylene blue (MB) degradation in aqueous solution under UV light.

Introduction

Considerable attention in crystalline functional coordination polymers (CPs) stems from their interesting topologies and potential applications in gas asorption and separation, catalysis, luminescence, magnetism, drug delivery, and so on.[1-3] As is well known, applications are determined by properties, which are essentially determined by structure. Thus, the design and syntheses of functional CPs remains a considerable challenge at this stage.[4,5]

Generally speaking, CPs are constructed form organic spacers (polycarboxylates, nitrogen heterocyclic linkers, organic phosphorus, and so on) and inorganic building blocks (metal ions, metal cluster, or secondary building units (SBUs)) under a given situation.[6,7] Hitherto, a great deal of aromatic polycarboxylates were extensively employed to construct multi-dimensional and functional CPs due to that the aromatic polycarboxylates can serve as excellent candidates for building highly connected, self-penetrating, or helical coordination frameworks for their bent backbones and versatile bridging fashions.[8] Apart from that the length, rigidity, coordination modes, functional groups, or substituents of organic acids have consequential effects on the final structures of MOFs.[9] Moreover, our previous researches proved that the stability of the frameworks can be enhanced by introducing the N-donors as the auxiliary ligands.[10-12] Moreover, the ancillary N−donor ligands also play an important role in adjusting the coordination mode of polycarboxylate acid, rarely documented to date.[13] The particular behaviors allow them to be promising candidates for designing beautiful frameworks with diverse topologies.

Based on the above mentioned points and following our recent research, two rectangular organic spacers (H_4tptc = terphenyl-3,3",5,5"-tetracarboxylic acid, H_4qptc = quaterphenyl-3,3'",5,5'"-tetracarboxylic acid) were employed to react with transition metal ions with the help of imidazole linkers, successfully obtained five CPs with distinct structures ranging from 3D (4,4)–connected 8^6 net (**4**), 3D (4,6)-connected $(4^2\cdot 6^4)(4^2\cdot 6^8\cdot 7\cdot 8^4)$ net (**1**), [Zn(1,3-bimb)] lock knots featured 2D+2D→3D entangled networks (**3** and **5**), to 2-fold 3D (3,3,4,4)-connected $(6\cdot 8^2)_2(6^2\cdot 8^3\cdot 10)(6^2\cdot 8^4)$ net (**2**). Besides, the luminescent properties of **4** and **5** have been investigated. Moreover, complexes **1-3** show relatively good photocatalytic activity for dye methylene blue (MB) degradation in aqueous solution under UV light.

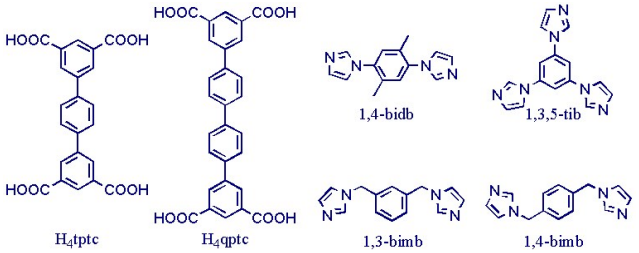

H_4tptc H_4qptc

Scheme 1. Structures of two tetracarboxylic acids and four ancillary imidazole ligands

[a] *State Key Laboratory of Crystal Materials, Shandong University , Jinan 250100, China. E-mail: xianzhao@sdu.edu.cn.*
[b] *Advanced Material Institute of Research, College of Chemistry and Chemical Engineering, Qilu Normal University, Jinan, 250013, China. E-mail: xiutangzhang@163.com.*

†Electronic Supplementary Information (ESI) available: Powder XRD patterns, TG curves, IR spectra, and X-ray crystallographic data, CCDC-1420870 for **1**, 1420871 for **2**, 1420872 for **3**, 923460 for **4**, and 923461 for **5**. See DOI: 10.1039/c5ce00000x.

Experimental Section

Materials and Methods. All chemical reagents were purchased from were purchased from Jinan Henghua Sci. & Tec. Co. Ltd. without further purification. IR spectra were measured on a NEXUS 670 FTIR spectrometer in the range of 600-4000 cm^{-1}. Elemental analyses were carried out on a CE instruments EA 1110 elemental analyzer. TGA was measured from 25 to 800 ^oC on a SDT Q600 instrument at a heating rate 5 ^oC/min under the N_2 atmosphere (100 mL/min). X-ray powder diffractions of **1**−**5** were measured and on a Panalytical X-Pert pro diffractometer with Cu-Kα radiation. Solid UV−visible spectra were obtained in the 200−800 nm range on a JASCOUVIDEC-660 spectrophotometer. Fluorescence spectra were performed on a Hitachi F-4500 fluorescence spectrophotometer at room temperature. Photocatalytic experiments in aqueous solutions were performed in a 30 mL test tube. A 125 W high-pressure mercury lamp was used as the UV light source. 1.0 mL 30% hydrogen peroxide was injected into 30 min dark adsorption pretreated 20.0 mL 2.5×10^{-5} mol L^{-1} methylene blue (MB) aqueous solution with 5 mg of powdered catalyst. At given irradiation time intervals, a series of aqueous solutions of a certain volume were collected and separated through a centrifuge to remove suspended catalyst particles and then subjected to UV−vis spectroscopic measurement.

General Synthesis Procedure for Complexes 1–5. Five CPs were synthesized under hydrothermal conditions and the oxalic acid act as the buffering agent in the formation of complex **2** and **3**. Moreover, other influences, such as metal ions, pH, and auxiliary ligands also plays an important role on adjusting the coordination modes of H_4tptc/H_4qptc as well as the final crystal packing structures. For **1**−**5**, the IR absorption bands around 3450 cm^{-1} can be attributed to the characteristic peaks of O-H vibrations. The vibrations at about 1400 cm^{-1} and 1610 cm^{-1} correspond to the asymmetric and symmetric stretching vibrations of the carboxyl groups, respectively (Fig. S1).[14]

Synthesis of $[Cu(H_2tptc)(1,4\text{-}bidb)]_n$ (1). A mixture of H_4tptc (0.15 mmol, 0.061 g), 1,4-bidb (0.20 mmol, 0.048 g), $CuCl_2\cdot2H_2O$ (0.30 mmol, 0.051 g), NaOH (0.30 mmol, 0.012g), and 12 mL H_2O was sealed in a 25 mL Teflon-lined stainless steel vessel, which was heated to 170 °C for 3 days and then cooled to room temperature slowly. Blue rodlike crystals of **1** were obtained. Yield 46% based on H_4tptc. Anal. (%) calcd. for $C_{36}H_{26}CuN_4O_8$: C, 61.23; H, 3.71; N, 7.93. Found: C, 61.45; H, 3.98; N, 8.07. IR (KBr pellet, cm^{-1}): 3643 (w), 3369 (w), 3132 (m), 2937 (s), 2165 (w), 1676 (w), 1592 (vs), 1575 (vs), 1536 (vs), 1514 (vs), 1421 (s), 1361 (vs), 1231 (s), 1045 (m), 776 (m).

Synthesis of $\{[Co_2(tptc)(1,3,5\text{-}tib)(H_2O)]\cdot7H_2O\}_n$ (2). A mixture of H_4tptc (0.15 mmol, 0.061 g), 1,3,5-tib (0.20 mmol, 0.055 g), $Co(NO_3)_2\cdot6H_2O$ (0.40 mmol, 0.116 g), Oxalic acid (0.30 mmol, 0.027 g), NaOH (0.30 mmol, 0.012 g), 13 mL H_2O and 2 mL EtOH was sealed in a 25 mL Teflon-lined stainless steel vessel, which was heated to 170 °C for 3 days and then cooled to room temperature slowly. Purple block crystals of **3** were obtained with the yield of 39% (based on H_4tptc). Anal. (%) calcd. for $C_{74}H_{58}Co_4N_{12}O_{25}$: C, 50.76; H, 3.34; N, 9.60. Found: C, 50.61; H, 3.32; N, 9.68. IR (KBr pellet, cm^{-1}): 3643 (w), 3123 (m), 1585 (m), 1540 (vs), 1422 (vs), 1371 (s), 1286 (m), 1141 (m), 862 (m), 848 (m), 744 (m).

Synthesis of $\{[Ni(tptc)_{0.5}(1,3\text{-}bimb)]\cdot H_2O\}_n$ (3). A mixture of H_4tptc (0.15 mmol, 0.061 g), 1,3-bimb (0.20 mmol, 0.048 g), $NiCl_2\cdot6H_2O$ (0.30 mmol, 0.071 g), Oxalic acid (0.30 mmol, 0.027 g), NaOH (0.40 mmol, 0.016 g), 13 mL H_2O and 2 mL DMF was sealed in a 25 mL Teflon-lined stainless steel vessel, which was heated to 170 °C for 3 days and then cooled to room temperature slowly. Green crystals of **3** were obtained. Yield 43% based on H_4tptc. Anal. (%) calcd. for $C_{25}H_{21}N_4NiO_5$: C, 58.17; H, 4.10; N, 10.85. Found: C, 57.96; H, 4.13; N, 10.81. IR (KBr pellet, cm^{-1}): 3058 (vs), 1981 (w), 1699 (w), 1608 (s), 1578 (s), 1542 (s), 1357 (vs), 1160 (m), 1017 (m), 977 (m), 827 (m), 762 (m).

Synthesis of $\{[Zn(qptc)_{0.5}(1,4\text{-}bimb)]\cdot3H_2O\}_n$ (4). A mixture of H_4qptc (0.15 mmol, 0.072 g), $Zn(OAc)_2\cdot2H_2O$ (0.30 mmol, 0.066 g), 1,4-bimb (0.30 mmol, 0.071 g), NaOH (0.60 mmol, 0.024 g), 8 mL H_2O and 8 mL EtOH was placed in a Teflon-lined stainless steel vessel, , which was heated to 170 °C for 3 days and then cooled to room temperature slowly. Colorless block crystals of **4** were obtained. Yield of 52% (based on H_4qptc). Anal. (%) calcd. for $C_{56}H_{54}N_8O_{14}Zn_2$: C, 56.34; H, 4.56; N, 9.39. Found: C, 56.30; H, 4.48; N, 9.27. IR (KBr pellet, cm^{-1}): 3139 (m), 2360 (m), 2324 (m), 1610 (m), 1558 (s), 1513 (vs), 1405 (s), 1352 (s), 1309 (s), 1252 (s), 1066 (s), 962 (m), 818 (s), 721 (m).

Synthesis of $\{[Zn(qptc)_{0.5}(1,3\text{-}bimb)]\cdot H_2O\}_n$ (5). The same synthetic procedure as for complex **4** was used except the 1,4-bimb was replaced by the 1,3-bmb. Colorless block crystals of **5** were obtained. Yield of 45% (based on H_4qptc). Anal. (%) calcd. for $C_{28}H_{23}N_4O_5Zn$: C, 59.96; H, 4.13; N, 9.99. Found: C, 59.92; H, 4.06; N, 9.89. IR (KBr pellet, cm^{-1}): 3368 (m), 1652 (s), 1590 (vs), 1561 (s), 1523 (s), 1382 (s), 1287 (s), 1214 (s), 1159 (m), 1006 (m), 858 (m), 744 (w).

X-ray crystallography. Intensity data collection was carried out on a Siemens SMART diffractometer equipped with a CCD detector using Mo-*Kα* monochromatized radiation (λ = 0.71073 Å). The absorption correction was based on multiple and symmetry-equivalent reflections in the data set using the SADABS program. The structures were solved by direct methods and refined by full-matrix least-squares using the SHELXTL package.[15] All non-hydrogen atoms were refined anisotropically. Hydrogen atoms except those on water molecules were generated geometrically with fixed isotropic thermal parameters, and included in the structure factor calculations. The SQUEEZE procedure was applied to eliminate the disordered solvent molecules of complexes **2**–**4**, and then the new files were generated. The hydrogen atoms attached to oxygen were refined with O–H=0.85Å and $U_{iso}(H) = 1.2U_{eq}(O)$. The carbon atoms in the phenyl rings of H_2tptc^{2-} ligands in complex **1** are disordered and refined with the occupancy ratio of 50:50 for C(16), C(17) and C(16A), C(17A), respectively. Crystallographic data for complexes **1**–**5** are given in Table 1. Selected bond lengths and angles for **1**–**5** are listed in Table S1. For complexes of **1**–**5**, further details of the crystal structure can be obtained from the http://www.ccdc.cam.ac.uk/deposit, on quoting the depository number CCDC-1420870 for **1**, 1420871 for **2**, 1420872 for **3**, 923460 for **4**, and 923461 for **5**.

Table 1 Crystal data for **1–5**

Compound	**1**	**2**	**3**	**4**	**5**
Empirical formula	$C_{36}H_{26}CuN_4O_8$	$C_{74}H_{44}Co_4N_{12}O_{18}$	$C_{25}H_{21}N_4NiO_5$	$C_{56}H_{42}N_8O_8Zn_2$	$C_{28}H_{23}N_4O_5Zn$
Formula weight	706.15	1624.93	516.17	1085.72	560.87
Crystal system	Monoclinic	Triclinic	Monoclinic	Monoclinic	Monoclinic
Space group	*C*2/*c*	*P*-1	$P2_1/n$	$P2_1/n$	$P2_1/n$
a (Å)	24.15(2)	11.573(3)	7.455(6)	9.3753(4)	8.928(2)
b (Å)	14.463(13)	13.892(4)	17.478(14)	16.5379(8)	16.369(4)
c (Å)	8.914(8)	14.655(4)	17.024(13)	18.0472(9)	17.650(4)
α (°)	90	62.631(4)	90	90	90
β (°)	90.251(16)	68.977(4)	101.686(13)	101.0940(10)	99.023(4)
γ (°)	90	68.800(4)	90	90	90
V(Å^3)	3113(5)	1897.2(8)	2172(3)	2745.9(2)	2547.5(10)
Z	4	1	4	2	4
D_{calcd} (Mg/m^3)	1.507	1.422	1.578	1.313	1.462
μ(mm^{-1})	0.764	0.935	0.941	0.933	1.011
T(K)	298(2)	293(2)	293(2)	296(2)	296(2)
R_{int}	0.0444	0.0313	0.0641	0.0277	0.0250
Final *R* indices[a]	0.0672 (0.1812)	0.0544 (0.1395)	0.0553 (0.1341)	0.0476 (0.1280)	0.0574 (0.1738)
R indices (all data)[a]	0.0914 (0.2004)	0.0830 (0.1533)	0.0931 (0.1506)	0.0706 (0.1359)	0.0866 (0.1937)
Gof	1.037	1.033	0.963	1.090	1.049

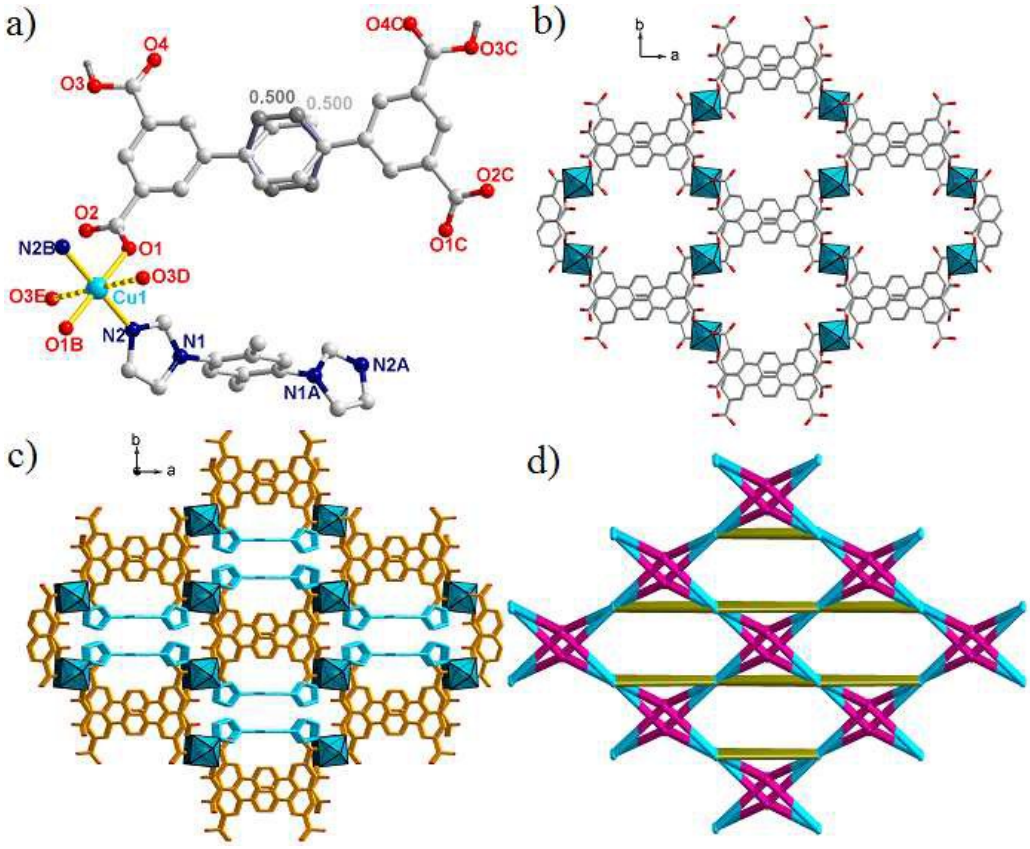

Figure 1. (a) Crystal structure of complex **1** (Symmetry codes: A: –*x*, *y*, –1/2–*z*; B: –*x*, *y*, 1/2–*z*; C: 1/2–*x*, 1/2–*y*, –*z*; D: 1/2–*x*, –1/2+*y*, 1/2–*z*; E: *x*, 1–*y*, –1/2+*z*.). (b) The 3D porous $[Cu_2(tptc)]_n$ networks view along *c* axis. (c) Schematic view of the 3D frameworks of **1**. (d) The unprecedented 3D (4,6)–connected $(4^2{\cdot}6^4)(4^2{\cdot}6^8{\cdot}7{\cdot}8^4)$ topology of **1** (green spheres: Cu ions, red spheres: $tptc^{4-}$ ligands, olive green bonds: 1,4-bib ligands).

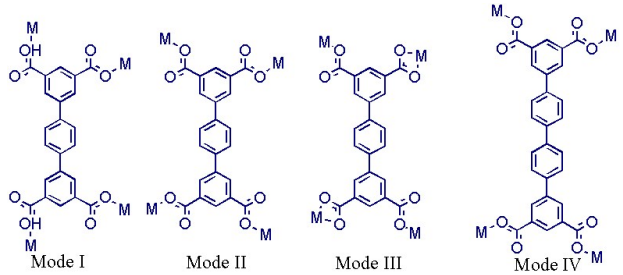

Scheme 2. The diverse coordination modes of two tetracarboxylic acids.

Result and Discussion

Structural Description of $[Cu(H_2tptc)(1,4\text{-bidb})]_n$ (1). Structural analysis reveals that complex **1** crystallizes in the monoclinic system, space group *C*2/*c*. As shown in Fig. 1a, the asymmetric unit consists of a half of Cu^{II} ion, a half of 1,4-bidb ligand, and a half of H_2tptc^{2-} ligands Each Cu^{II} ion lies on an inversion centre of a planar quadrilateral geometry (with the τ_4 parameter is 0), tetra-coordinated by two carboxyl O atoms from two H_2tptc^{2-} ligands and two N atoms from two 1,4-bidb ligands.

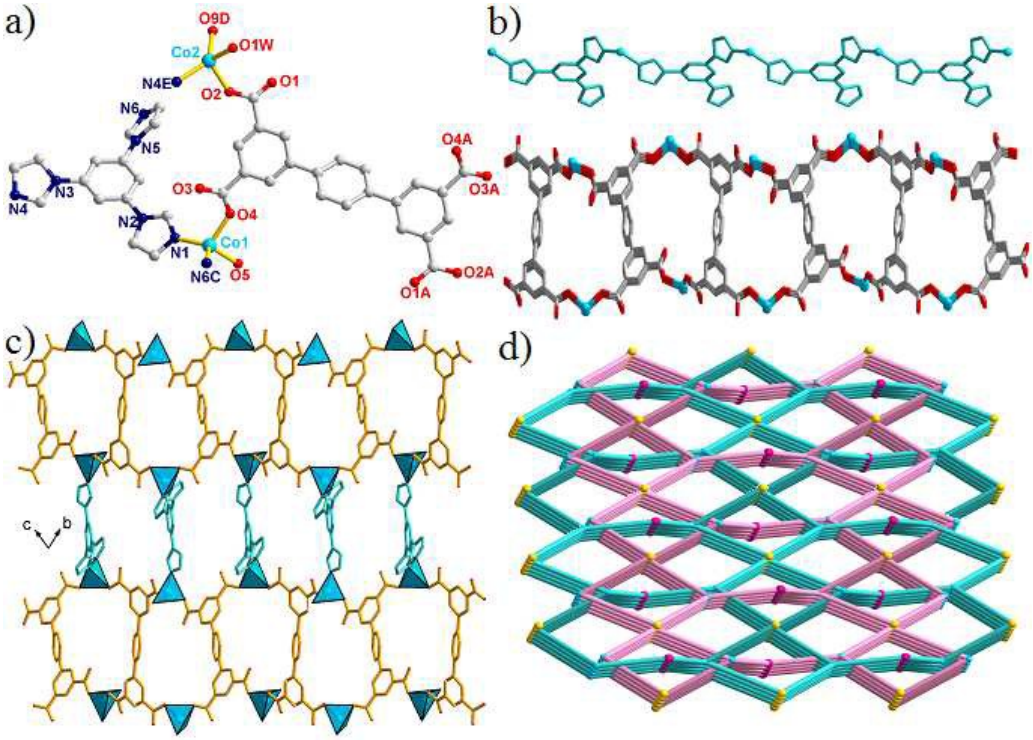

Figure 2. (a) Crystal structure of complex **2** (Symmetry codes: A: –*x*, 2–*y*, 1–*z*; C: –1+*x*, *y*, *z*; D:1+*x*, 1+*y*, –1+*z*; E: 2–*x*, 1–*y*, –*z*.). (b) The 1D $[Co(1,3,5\text{-}tib)_3]_n$ chain (the above) and $[Co_2(tptc)]_n$ bilayer (the below). (c) The 3D porous frameworks of **3** views along *a* direction. (d) The interesting 2-fold interpenetrated framework with the (3,3,4,4)-connected $(6\cdot8^2)_2(6^2\cdot8^3\cdot10)(6^2\cdot8^4)$ topology for **2**.

In **1**, H_4tptc is partially deprotonated and linked two Cu^{II} ions through the monodentate carboxyl groups. The other two protonated carboxyl groups have strong interactions with the Cu^{II} ions (Cu-O3D=2.764(5) Å). Thus, the H_2tptc^{2-} can be view as a four-connected node with $(\kappa^1\text{-}\kappa^0)\text{-}(\kappa^0\text{-}\kappa^1)\text{-}(\kappa^0\text{-}\kappa^1)\text{-}(\kappa^1\text{-}\kappa^0)\text{-}\mu_4$ coordination mode (Mode I, Scheme 2). Cu^{II} ions are connected by H_2BDP^{2-} to form a 3D $[Cu(H_2tptc)]_n$ framework consisting of 1D channels with 12.952(5) × 8.540(9) $Å^2$ openging along *c* axis (Fig. 1b). Then the 1D $[Cu(1,4\text{-}bidb)]_n$ chains (Fig. S2) occupied those 1D channels *via* connecting adjacent Cu^{II} ions, finally given 3D net (Fig. 1c). Topology analysis shows that the overall network of **1** features a new 3D (4,6)–connected net with the Schläfli symbol of $(4^2\cdot6^4)(4^2\cdot6^8\cdot7\cdot8^4)$ by denoting the H_2tptc^{2-} ligands as 4–connected nodes, and Cu^{II} ions as 6–connected nodes, respectively (Fig. 1d).[16]

Structural Description of $\{[Co_2(tptc)(1,3,5\text{-}tib)(H_2O)]\cdot7H_2O\}_n$ (2). Structural analysis reveals that complex **2** crystallizes in the monoclinic space group $P2_1/n$. The asymmetric unit consists of two Co^{II} ions, one $tptc^{4-}$, one 1,3,5-tib ligand, one coordinated, and seven lattice water molecules (Fig. 2a). Co (1) is tetracoordinated by two O atoms from two different $tptc^{4-}$ ligands and two N atoms from two different 1,3,5-tib linkers, exhibiting a distorted tetrahedral geometry (τ_4 = 0.88(8)). Co (2) locates in a similar tetrahedral $[CoNO_3]$ coordination environment with the τ_4 parameter being 0.79(8), completed by two O atoms from two $tptc^{4-}$ ligands, one O atom from the associated water molecule, and one N atom from one 1,3,5-tib ligand. Besides, the Co-O/N bond lengths span in the range of 1.935(1)-2.023(5) Å, respectively.

The completely deprotonated $tptc^{4-}$ exhibits $(\kappa^1\text{-}\kappa^0)\text{-}(\kappa^1\text{-}\kappa^0)\text{-}(\kappa^1\text{-}\kappa^0)\text{-}(\kappa^1\text{-}\kappa^0)\text{-}\mu_4$ coordination mode (Mode II) and coordinates four cobalt ions to form a 2D $[Co_2(tptc)]_n$ bilayer with 1D semicircle channels (diameter is about 11.366(4) Å) (Fig. 2b). While the tripodal 1,3,5-tib acts as the μ_3-bridge to connect adjacent Co ions through imidazole N atoms, finally resulting in a 1D $[Co(1,3,5\text{-}tib)]_n$ chain with the Co(1)···Co(1) distance being 11.573(0) Å (Fig. 2b). Then the 1D $[Co(1,3,5\text{-}tib)]_n$ chains hinged the neighbouring 2D $[Co_2(tptc)]_n$ bilayers together, finally exhibiting a porous network with two kinds of channels along *a* axis (Fig. 2c). Two adjacent networks interacted with each other through the hydrogen bonds, which make the interpenetrated supramolecular more stable (Fig. S3).

Topology analysis reveals that complex **2** is a 3D 2-fold interpenetrated framework with the unprecedented (3,3,4,4)-connected $(6\cdot8^2)_2(6^2\cdot8^3\cdot10)(6^2\cdot8^4)$ topology by simplifying 1,3,5-tib and Co(2) as 3–connected nodes, and Co(1) and $tptc^{4-}$ ligands as 4–connected nodes, respectively (Fig. 2d).

Structural Description of $\{[Ni(tptc)_{0.5}(1,3\text{-}bimb)]\cdot H_2O\}_n$ (3). Complex **3** crystallizes in the monoclinic system $P2_1/n$. As shown in Fig. 3a, there are one crystallographically independent Ni^{II} ion, a half of central symmetry $tptc^{4-}$ ligand, one 1,3-bimb ligand, and one lattice water molecule in the asymmetric unit. Ni^{II} is pentacoordinated by two N atoms from two 1,3-bimb ligands, and three O atoms from two $tptc^{4-}$ ligands, exhibiting a distorted square pyramidal coordination geometry with τ_5 = 0.07(0).

In the formation of complex **3**, the completely deprotonated $tptc^{4-}$ ligand shows $(\kappa^1\text{-}\kappa^1)\text{-}(\kappa^0\text{-}\kappa^1)\text{-}(\kappa^1\text{-}\kappa^1)\text{-}(\kappa^0\text{-}\kappa^1)\text{-}\mu_4$ coordination mode (Mode III) linking four Ni^{II} ions, finally leading to a 2D $[Ni_2(qptc)]_n$ sheet (Fig. 3b). Beside, the Ni^{II}

ions are bridged by 1,3-bimb linkers to result in a 1D [Ni(1,3-bimb)]$_n$ snake chain, which can be defined as a single left- or right-handed helix with the Ni···Ni distance being 8.711(4) Å (Fig. S4). The [Ni_2(qptc)]$_n$ sheet cooperated with the 1D [Ni(1,3-bimb)]$_n$ snake chain, finally showing a 2D sheet (Fig. 3c). It is noteworthy that the adjacent sheets interact with each other through the "lock knot" structure, finally leaving a 2D→3D entangled network (Fig. S5). From the topology viewpoint, the whole structure of complex **3** can be defined as a **kgm** sheet entangled network (Fig. 3d).

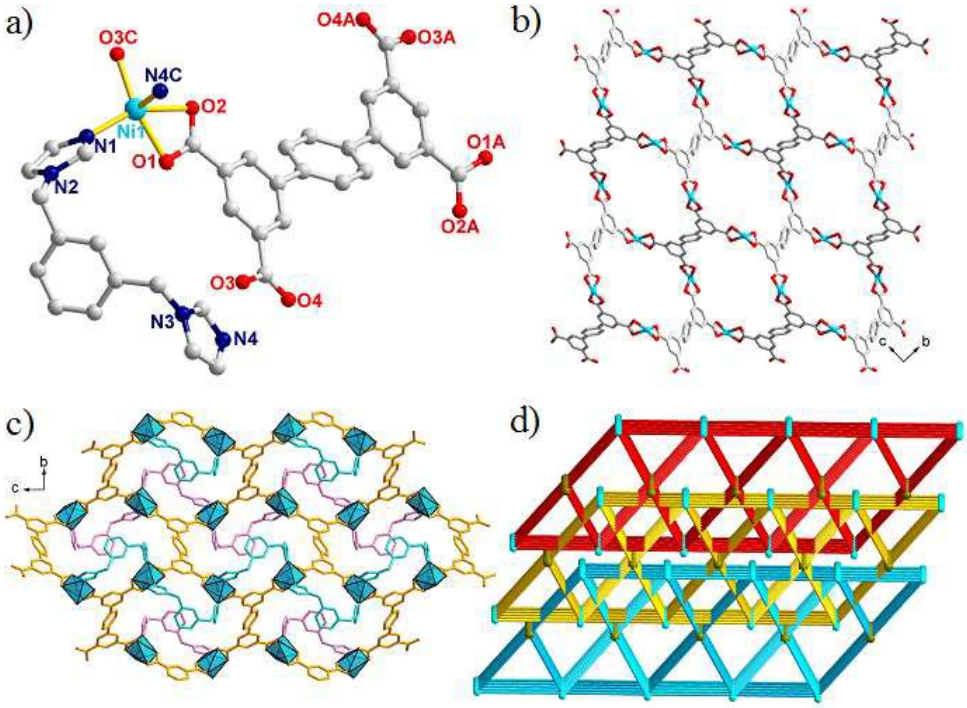

Figure 3. (a) Crystal structure of complex **3** (Symmetry codes: A: 3–*x*, 1–*y*, 1–*z*; C: 1/2+*x*, 3/2–*y*, 1/2+*z*.). (b) The 2D [Ni_2(tptc)]$_n$ layer view along *a* direction. (c) Schematic view of the 2D sheet of **3** along *a* direction. (d) ($3^2 \cdot 6^2 \cdot 7^2$)-**kgm** sheet entangled 3D packing supramolecular structure of **3**.

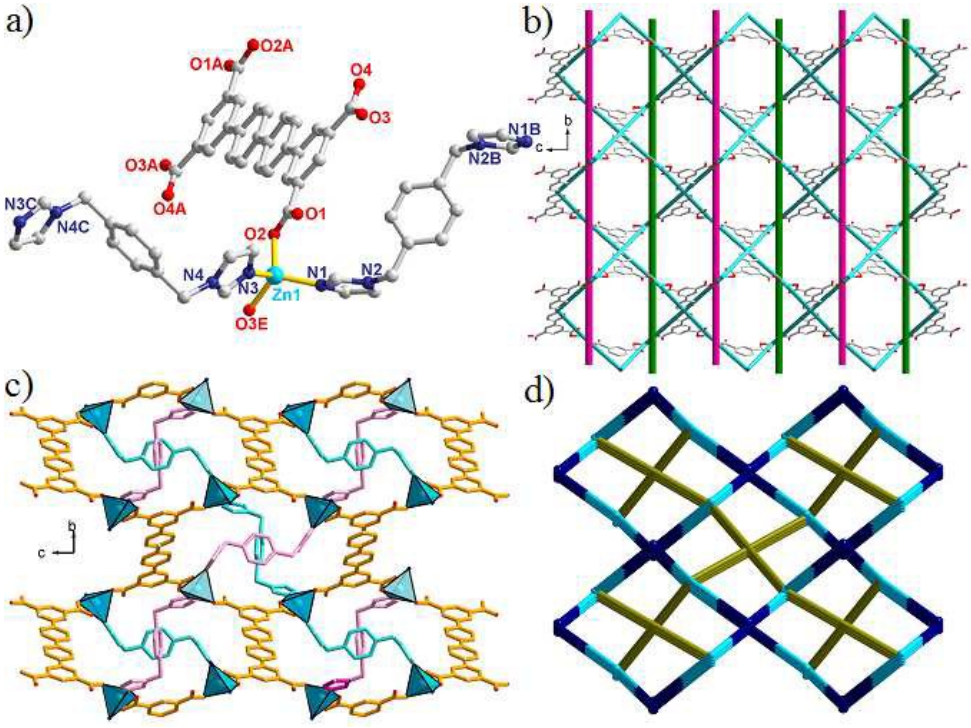

Figure 4. (a) Crystal structure of complex **4** (Symmetry codes: A: –*x*, –*y*, 1–*z*;; B: 2–*x*, 1–*y*, 1–*z*; C: 2–*x*, –*y*, –*z*; E: –1/2+*x*, 1/2–*y*, –1/2+*z*.). (b) The 2D [Zn_2(qptc)]$_n$ network with right- and left- handed helix chains. (c) Schematic view of the 3D frameworks of **4** along *a* direction. (d) The novel 3D (4,4)–connected 8^6 net of **4** (green spheres: Zn ions, dark blue spheres: $qptc^{4-}$ ligands, olive green bonds: 1,4-bimb ligands).

Structural Description of $\{[Zn(qptc)_{0.5}(1,4\text{-bimb})]\cdot 3H_2O\}_n$ (4). Single-crystal X-ray analysis reveals that **4** crystallizes in monoclinic system, *P2/n* space group and the asymmetric unit consists of one Zn^{II} ion, a half of $qptc^{4-}$ ligand which lying about independent inversion centre, one 1,4-bimb ligand, and three lattice water molecules (Fig. 4a). Each Zn^{II} ion is tetracoordinated with two O atoms from two different $qptc^{4-}$ ligands, and two N atoms from two different 1,4-bimb linkers, exhibiting distorted tetrahedral coordination geometry (τ_4 = 0.92(4)). The Zn-O/N bond lengthes are in the range of 1.9592(18)- 2.0175(19) Å.

The H_4qptc ligand is completely deproponated in complex **4** and linked four Zn^{II} ions *via* its four monodentate carboxyl groups, resulting in a 2D $(4^4\cdot6^2)$-**sql** $[Zn(qptc)_{0.5}]_n$ sheet with right- and left- handed helixes alternately arranged (Fig. 4b). And the Zn^{II} ions bridged by the 1,4-bimb linkers, successfully constructed a 1D $[Zn(1,4\text{-bimb})]_n$ wave chain, with the 1,4-bimb separated Zn···Zn distance are 13.920(5) and 14.552(8) Å (Fig. S6). Sharing the Zn^{II} ions, the 2D $[Zn(qptc)_{0.5}]_n$ sheets worked with the 1D $[Zn(1,4\text{-bimb})]_n$ wave chains, successfully generated an unprecedented (4,4)-connected net with the Schläfli symbol of 8^6 by denoting both the $qptc^{4-}$ ligands and Zn^{II} ions to 4−connected nodes (Fig. 4d).

Structural Description of $\{[Zn(qptc)_{0.5}(1,3\text{-bimb})]\cdot H_2O\}_n$ (5). Complex **5** was obtained under similar reaction conditions of **4**. When the longer 1,4-bimb was replaced by the 1,3-bimb, the final obtained structures degraded from the 3D (4,4)-connected 8^6 net to the 2D 4–connected $(3^2\cdot6^2\cdot7^2)$-**kgm** sheet. Structural analysis reveals that complex **5** crystallizes in the monoclinic system, *P2/n* space group. There are one crystallographically independent Zn^{II} cation, a half of $qptc^{4-}$, one 1,3-bimb, and one lattice water molecule in the asymmetric unit. Shown in Fig. 5a, the Zn^{II} ion located in a distorted tetrahedral coordination geometry (τ_4 = 0.91(7)), completed by two O atoms form two $qptc^{4-}$ ligands and two N atoms from two 1,3-bimb linkers.

In complex **5**, the coordination mode of $qptc^{4-}$ is same with that in complex **4**, and the $qptc^{4-}$ ligands linked the Zn^{II} ions, forming a similar 2D $[Zn(qptc)_{0.5}]_n$ sheet with a much bigger square (16.342×16.533 Å). And the 1,3-bimb act as the bridging linkers, linking the neighbouring Zn^{II} ions, finally formed a 2D $[Zn(qptc)_{0.5}]_n$ sheet (Fig. 5b), in which the 1,3-bimb separated Zn···Zn distance is 9.397(1) Å (Fig. S7). In the topology opinion, the sheet can be simplified to be a 4–connected $(3^2\cdot6^2\cdot7^2)$-**kgm** net (Fig. 5c). The adjacent sheets can be further expanded to be a 2D→3D entangled networks through the "lock knot" structures (Fig. 5d).

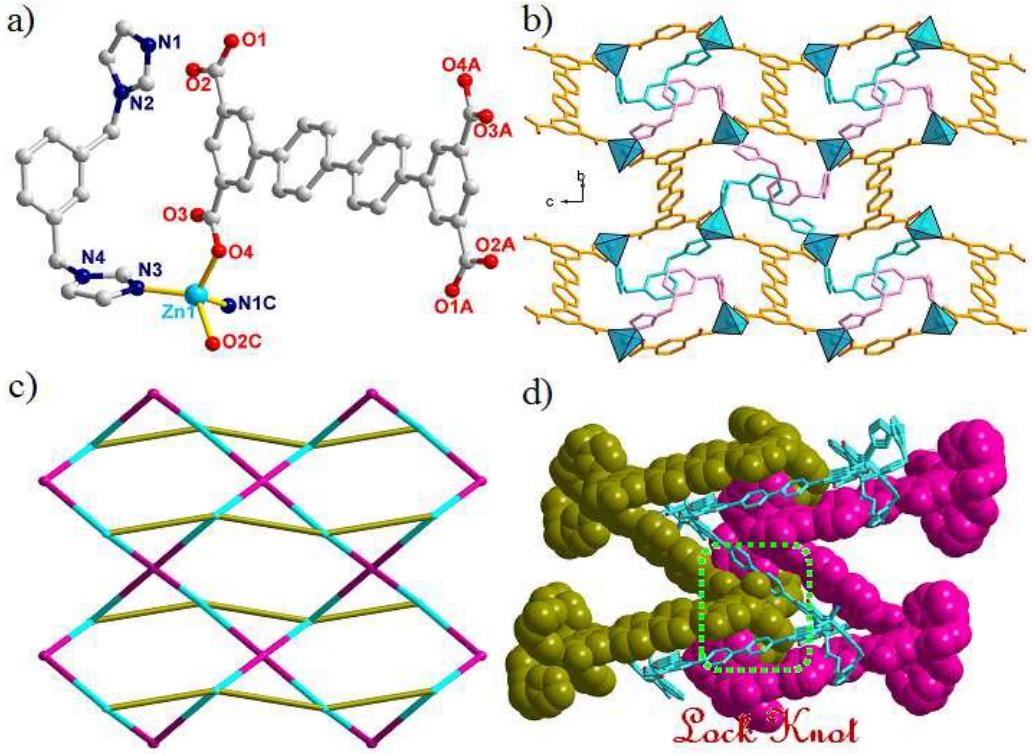

Figure 5. (a) Crystal structure of complex **5** (Symmetry codes: A: –1–*x*, –*y*, 1–*z*; C: –1/2+*x*, 1/2–*y*, –1/2+*z*.). (b) The 2D sheet of complex **5** view along *a* direction. (c) The 2D 4–connected $(3^2\cdot6^2\cdot7^2)$-**kgm** sheet of **5** (green spheres: Zn ions, red spheres: $qptc^{4-}$ ligands, olive green bonds: 1,3-bimb ligands). (d) The 3D supramolecular structure featured by the sheets hinged together through the lock knots.

Table 2 The detailed comparisons of complexes **1**–**5**.

	Coord.Modes	H_xt(q)ptc motifs	τ_4 or τ_5 parameter [a]	Final Structure and Topology
1	Mode I	3D $[Cu(H_2tptc)]_n$ net	τ_4 = 0 for Cu1	3D (4,6)-connected $(4^2\cdot6^4)(4^2\cdot6^8\cdot7\cdot8^4)$ net
2	Mode II	2D $[Co_2(tptc)]_n$ bilayer	τ_4 = 0.88(8) for Co1, τ_4 =0.79(8) for Co2	2-fold 3D (3,3,4,4)-connected $(6\cdot8^2)_2(6^2\cdot8^3\cdot10)(6^2\cdot8^4)$ net
3	Mode III	2D $[Ni_2(tptc)]_n$ sheet	τ_5 = 0.07(0) for Ni1	2D 4-connected $(3^2\cdot6^2\cdot7^2)$-**kgm** sheet
4	Mode IV	2D $[Zn_2(qptc)]_n$ sheet	τ_4 = 0.92(4) for Zn1	3D (4,4)–connected 8^6 net
5	Mode IV	2D $[Zn_2(qptc)]_n$ sheet	τ_4 = 0.91(7) for Zn1	2D 4-connected $(3^2\cdot6^2\cdot7^2)$-**kgm** sheet

[a] $\tau_4 = [360°-(\alpha+\beta)]/141°$; $\tau_5 = |\beta-\alpha|/60°$; α and β are the two largest bond angles in the four or five-coordinate complex.

Syntheses and Structural Comparison. As shown in Scheme 2, in complex **1-5**, the deproponated H_4tptc/H_4qptc ligands all act as μ_4 linkers, connecting four metal ions with monodentate or cheating carboxyl groups, and thus resulted in 2D $[M(tptc)]_n$ or 2D $[M(qptc)]_n$ sheets. The metal ions as well as the imidazole auxiliary linkers have great influences on the assembly of the final structures: i) the τ_4 (τ_4 = [360°-(α+β)]/141°) or τ_5 (τ_5 =|β-α|/60°) parameter of metal ions (Table 2), for four-coordinated metal ions (**1**, **2**, **4**, and **5**), the Cu^{II} in complex **1** lies in a planar quadrilateral geometry with τ_4 = 0, indicting the expanded direction along a plane, rather than the space expanded for **2**, **4**, and **5**. And the Ni^{II} in complex **3** lies in a square pyramidal coordination geometry (τ_5 = 0.07(0)), which proved the expanded direction is three dimensional; ii) the imidazole auxiliary linkers act as the bridging or tripodal linkers, holding distinct lengths, coordination modes and flexibilities, adjust themselves by rotating, folding, twisting to satisfy the coordination preferences of different metal ions, given 1D flat $[Cu(1,4\text{-bidb})]_n$ chain for **1**, 1D zigzag $[Co(1,3,5\text{-tib})]_n$ chain for **2**, 1D double helix $[Ni(1,3\text{-bimb})]_n$ chain for **3**, 1D wave $[Zn(1,4\text{-bimb})]_n$ chain for **4**, and 1D double helix $[Zn(1,3\text{-bimb})]_n$ chain for **5**. The synergistic effects of two rectangular organic spacers and imidazole auxiliary linkers make the five CPs obtained, in which a systematic variation exhibited from 3D (4,4)–connected 8^6 net (**4**), 3D (4,6)-connected $(4^2\cdot6^4)(4^2\cdot6^8\cdot7\cdot8^4)$ net (**1**), [Zn(1,3-bimb)] lock knots featured 2D+2D→3D entangled networks (**3** and **5**), to 2-fold 3D (3,3,4,4)-connected $(6\cdot8^2)_2(6^2\cdot8^3\cdot10)(6^2\cdot8^4)$ net (**2**).

X-ray Power Diffraction Analyses and Thermal Analyses. In order to check the phase purity of these complexes, the PXRD patterns of title complexes were checked at room temperature. As shown in Fig. S8, the peak positions of the simulated and experimental PXRD patterns are in agreement with each other, demonstrating the good phase purity of the complexes, and the differences of the PXRD patterns may be due to the preferred orientation of the crystalline powder sample. The experiments of thermogravimetric analysis (TGA) were performed on samples of **1-5** under N_2 atmosphere with a heating rate of 10 °C min^{-1}, shown in Fig. S9. For complex **1**, the networks remains stable until the temperature up to 320 °C, finally the complex was pyrolyzed with a result of thermal decomposition. For complex **2**, the first weight loss at about 100 °C can be attributed to the release of coordinated and lattice water molecules (obsd: 6.3%; calcd: 6.2%). And the second weight loss around 380 °C corresponds to the loss of the organic ligands, finally given some unknown powder. There are also two main stages of weight loss in the sample collapses of complex **3**. The first weight loss of 3.71 % below 100 °C is ascribed to the release of lattice water molecules (3.49 %). And then the frameworks exist stably below 350 °C. Above this temperature, the net collapsed with both the $tptc^{4-}$ and 1,3-bimb released. In the case of complex **4**, the weight loss of 8.83 % from 70 to 150°C is attributed to the loss of lattice water molecules (calc. 9.05 %). The weight loss corresponding to the release of organic ligands starts at 340°C with a result of thermal decomposition. For complex **5**, the lattice water molecules loss around 100°C, with the weight loss of 4.96 % (calc. 4.73 %). And then the organic pillars of the frameworks begin to pyrolyze when the temperature up to 360 °C, finally given a result of thermal decomposition.

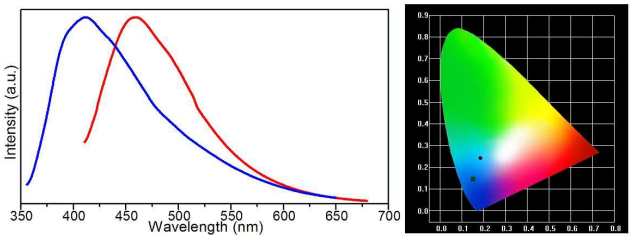

Figure 6. Emission spectra of complexes **4** (blue) and **5** (red) in the solid state at room temperature (The insert CIE, (0.17, 0.23) for **4**, and (0.15, 0.14) for **5**).

Photoluminescent Properties. The fluorescence spectrum of **4** and **5** were examined in the solid state at room temperature, shown in Fig. 6 after normalized. It can be observed that intense emissions occur at 458 nm (λ_{ex} = 394 nm) for **4**, and 410 nm (λ_{ex} = 342 nm) for **5**, respectively. The emission is neither metal-to-ligand charge transfer (MLCT) nor ligand-to-metal transfer (LMCT) in nature since the Zn^{II} ion is difficult to oxidize or reduce due to its d^{10} configuration.[17] Thus, they can be assigned to intraligand ($\pi^*\rightarrow n$ or $\pi^*\rightarrow\pi$) emission. As illustrated by the CIE (CIE = Commission International de l'Echairage) chromaticity coordinates of the emission spectra in Fig. 6, the overall emission is located in the cyan region with CIE chromaticity coordinate of (0.17, 0.23) for **4**, and blue region with CIE chromaticity coordinate of (0.15, 0.14) for **5**, respctively. The observation indicates that the polymeric complexes of **4** and **5** may be excellent candidate for the efficient blue emission material.

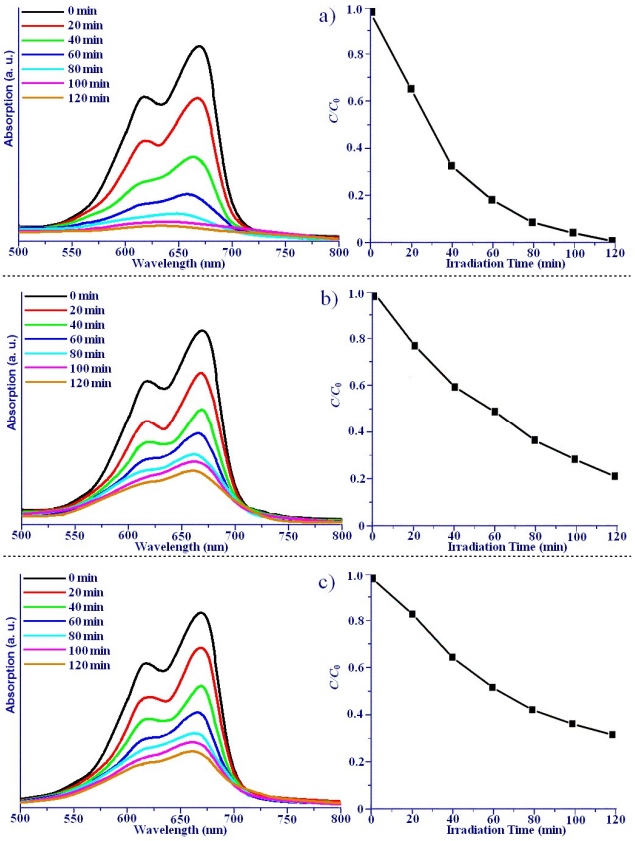

Figure 7. UV-Vis absorption spectra of the MB solutions degraded by different photocatalysts under UV irradiation at different time intervals: (a) **1** in MB; (d) **2** in MB; and (c) **3** in MB.

Photocatalytic Investigation. As we all known, in the coordination architectures, the redox properties of the central metal ions directly determines the efficiency of photocatalysis. The diffuse-reflectance UV-vis spectra reveal the absorption features of complexes **1**–**3** (Fig. S10), and all spectra consist of absorption components in the UV region. The main intense absorption peaks at 283, 257, and 267 nm for **1**, **2**, and **3**, which can be attributed to π–π* transitions of the organic ligands. It should be noted that the charge-transfer transition of complexes **1**–**3** occurs in the UV region, which may be given a higher photocatalytic activity with UV-light.[18] Hence, we selected fresh prepared complexes **1-3** as the catalysts evaluate the photocatalytic activities in the purification of Methylene blue (MB), because the Zn^{II} ion is difficult to oxidize or reduce due to its d^{10} configuration. The decomposition of dye methylene blue (MB) was monitored by the characteristic absorption band at 665 nm. As illustrated in Fig. 7, changes in the concentration of MB solution were plotted versus irradiation time. The calculation results show that the degradation efficiency of MB is upto 97.3 % after 2 hours for **1**, 77.4 % for **2**, 66.8 % for **3**, respectively. Under the same conditions, the total catalytic degradation efficiencies of the control experiments under dark and under illumination (without catalyst) after 2 hours are 9.6 % and 28.7 %, respectively (Fig. S11). The photocatalystic investigation shows complex **1** exhibiting relatively good photocatalytic activity than complex **2** and **3** for dye methylene blue (MB) degradation in aqueous solution under UV light, which indicating different metal ions holding distinct photocatalytic activities for their redox properties.[19] The possible mechanism for the MB degradation is proposed as described in the previous literature.[20] Under the irradiation of UV-Vis light, the organic ligands were induces to produce O or N-metal charge transfer promoting electrons from the highest occupied molecular orbital (HOMO) to the lowest unoccupied molecular orbital (LUMO). Therefore, the HOMO strongly needs one electron to return to its stable state. Thus, one electron was captured from water molecules, which was oxygenated to generate the ·OH radicals. And then the ·OH active species could decompose the MB effectively to complete the photocatalytic process.

Conclusions

In summary, we successfully obtained five CPs with distinct structures ranging from 3D (4,4)–connected 8^6 net (**4**), 3D (4,6)-connected $(4^2{\cdot}6^4)(4^2{\cdot}6^8{\cdot}7{\cdot}8^4)$ net (**1**), [Zn(1,3-bimb)] lock knots featured 2D+2D→3D entangled networks (**3** and **5**), to 2-fold 3D (3,3,4,4)-connected $(6{\cdot}8^2)_2(6^2{\cdot}8^3{\cdot}10)(6^2{\cdot}8^4)$ net (**2**) by using two rectangular tetracarboxylates and the imidazole linkers. This study broadens the exploration of the synthetic strategy on CPs construction. The solid-state photoluminescent studies revealed that **4** and **5** exhibit strong blue emission mainly originating from charge transfer between the delocalized π bonds of the aromatic ligands. Moreover, complexes **1-3** shows relatively good photocatalytic activity for dye methylene blue (MB) degradation in aqueous solution under UV light.

Acknowledgements. The work was supported by financial support from the Natural Science Foundation of China (Grant Nos. 21101097, 21451001), key discipline and innovation team of Qilu Normal University.

Notes

The authors declare no competing financial interest.

References

1. (a) A. Dhakshinamoorthy, A. M. Asiri and H. Garcia, *Chem. Soc. Rev.*, 2015, **44**, 1922; (b) T. R. Cook, Y. R. Zheng and P. J. Stang, J. *Chem. Rev.*, 2013, **113**, 734; (c) D. S. Li, Y. P. Wu, J. Zhao, J. Zhang and J. Y. Lu, *Coord. Chem. Rev*., 2014, **261**, 1; (d) G. Férey and C. Serre, *Chem. Soc. Rev*., 2009, **38**, 1380; (e) A. Mallick, B. Garai, M. A. Addicoat, P. S. Petkov, T. Heine and R. Banerjee, *Chem. Sci.*, 2015, **6**, 1420.
2. (a) D. B. Shinde, S. Kandambeth, P. Pachfule, R. R.Kumar and R. Banerjee, *Chem. Commun.*, 2015, **51**, 310; (b) E. D. Bloch, W. L. Queen, R. Krishna, J. M. Zadrozny, C. M. Brown and J. R. Long, *Science*, 2012, **335**, 1606; (c) A. Goeppert, M. Czaun, J. Jones, G. K. S. Prakash and G. A. Olah, *Chem. Soc. Rev.*, 2014, **43**, 7995; (d) X. T. Zhang, D. Sun, B. Li, L. M. Fan, B. Li and P. H. Wei, *Cryst. Growth Des.*, 2012, **12**, 3845; (e) T. Panda, K. M. Gupta, J. Jiang and R. Banerjee, *CrystEngComm*, 2014, **16**, 4677.
3. (a) V. Guillerm, D. Kim, J. F. Eubank, R. Luebke, X. Liu, K. Adil, M. S. Lah and M. Eddaoudi, *Chem. Soc. Rev.*, 2014, **43**, 6141; (b) J. B. Lin, W. Xue, B. Y. Wang, J. Tao, W. X. Zhang, J. P. Zhang and X. M. Chen, *Inorg. Chem*., 2012, **51**, 9423; (c) X. Zhang, L. Fan, W. Zhang, Y. Ding, W. Fan and X. Zhao, *Dalton Trans.,* 2013, **42**, 16562; (d) Q. Zhang, H. Zhang, S. Zeng, D. Sun and C. Zhang, *Chem-Asian J.*, 2013, **8**, 1985; (e) U. P. Singh, S. Narang, P. Pachfule and R. Banerjee, *CrystEngComm*, 2014, **16**, 5012.
4. (a) W. L. Leong and J. J.Vittal, *Chem. Rev*., 2011, **111**, 688; (b) A. Schneemann, V. Bon, I. Schwedler, I. Senkovska, S. Kaskel and R. A. Fischer, *Chem. Soc. Rev.*, 2014, **43**, 6062; (c) X. H. Chang, Y. Zhao, M. L. Han, L. F. Ma and L. Y. Wang, *CrystEngComm*, 2014, **16**, 6417; (d) W. Shi, S. Song and H. Zhang, *Chem. Soc. Rev*., 2013, **42**, 5714; (e) C. Dey and R. Banerjee, *Chem. Commun*., 2013, **49**, 6617.
5. (a) P. Pachfule, S. Kandambeth, D. D. Díaz and R. Banerjee, *Chem. Commun.*, 2014, **50**, 3169; (b) U. J. Williams, B. D. Mahoney, A. J. Lewis, P. T. DeGregorio, P. J. Carroll and E. J. Schelter, *Inorg. Chem.*, 2013, **52**, 4142; (c) M. L. Han, X. C. Chang, X. Feng, L. F. Ma and L. Y. Wang, *CrystEngComm*, 2014, **16**, 1687; (d) K. Su, F. Jiang, J. Qian, L. Chen, J. Pang, S. M. Bawaked, M. Mokhtar, S. A. Al-Thabaiti and M. Hong, *Inorg. Chem.,* 2015, **54**, 3183.
6. (a) A. Aijaz, J. -K. Sun, P. Pachfule, T. Uchida and Q. Xu, *Chem. Commun.*, 2015, **51**, 13945; (b) L. Fan, X. Zhang, D. Li, D. Sun, W. Zhang and J. Dou, *CrystEngComm*, 2013, **15**, 349; (c) L. P. Xue, C. X. Chang, S. H. Li, L. F. Ma and L. Y. Wang, *Dalton Trans.,* 2014, **43**, 7219; (d) L. L. Liu, C. X. Yu, J. Sun, P. P. Meng, F. J. Ma, J. M. Du and L. F. Ma, *Dalton Trans.,* 2014, **43**, 2915; (e) B. Bhattacharya, D. K. Maity, P. Pachfule, E. Colacio and D. Ghoshal, *Inorg. Chem. Front.*, 2014, **1**, 414.
7. (a) S. Dutta, D. -K. Bučar, E. Elacqua and L. R. MacGillivray, *Chem. Commun.*, 2013, **49**, 1064; (b) X. Zhang, L. Fan, W. Zhang, W. Fan, L. Sun and X. Zhao, *CrystEngComm*, 2014, **16**, 3203; (c) L. Fan, W. Fan, B. Li, X. Liu, X. Zhao and X. Zhang, *Dalton Trans.*, 2015, **44**, 2380; (d) X. Zhang, L. Fan, Z. Sun, W. Zhang, W. Fan, L. Sun and X. Zhao, *CrystEngComm*, 2013, **15**, 4910; (e) M. Meng, D. C. Zhong and T. B. Lu, *CrystEngComm*, 2011, **13**, 6794.
8. (a) R. E. Osta, M. Frigoli, J. Marrot, N. Guillou, H. Chevreau, R. I. Walton and F. Millange, *Chem. Comm.*, 2012, **48**, 10639; (b) J. Zhao, D. S. Li, X. J. Ke, B. Liu, K. Zou and H. M. Hu, *Dalton Trans.,* 2012, **41**, 2560; (c) W. Liu, L. Ye, X. Liu, L. Yuan, J. Jiang and C. Yan, *CrystEngComm*, 2008, **10**, 1395; (d) M. Yan, F. Jiang, Q. Chen, Y. Zhou, R. Feng, K. Xiong and C. Hong, *CrystEngComm*, 2011, **13**, 3971.
9. (a) X. Lin, J. Jia, X. Zhao, K. M. Thomas, A. J. Blake, G. S. Walker, N. R. Champness, P. Hubberstey and M. Schrder, *Angew. Chem. Int. Ed.*, 2006, **45**, 7358; (b) F. Guo, B. Zhu, M. Liu, X. Zhang, J. Zhang

and J. Zhao, *CrystEngComm*, 2013, **15**, 6191; (c) H. R. Fu, F. Wang and J. Zhang, *Dalton Trans.,* 2014, **43**, 4668; (d) T. Panda, P. Pachfule and R. Banerjee, *Chem. Commun.*, 2011, **47**, 7674.

10. (a) H. Deng, S. Grunder, K. E. Cordova, H. Furukawa, M. Hmadeh, F. Gandara, A. C. Whalley, Z. Liu, S. Asahina, H. Kazumori, M. O'Keefee, O. Terasaki, J. F. Stoddart and O. M. Yaghi, *Science*, 2012, **336**, 1018; (b) L. F. Ma, Z. Z. Shi, F. F. Li, J. Zhang and L. Y. Wang, *New J. Chem.*, 2015, **39**, 810; (c) J. Yang, X. Wang, F. Dai, L. Zhang, R. Wang and D. Sun, *Inorg. Chem.,* 2014, **53**, 10649; (d) J. H. Qin, L. F. Ma, Y. Hu and L. Y. Wang, *CrystEngComm*, 2012, **14**, 2891.

11. (a) Y. Mu, G. Han, S. Ji, H. Hou and Y. Fan, *CrystEngComm*, 2011,**13**, 5943; (b) Fan, W. Fan, W. Song, G. Liu, X. Zhang and X. Zhao, *CrystEngComm*, 2014, **16**, 9191; (c) L. Chen, L. Zhang, S. L. Li, Y. Q. Qiu, K. Z. Shao, X. L. Wang and Z. M. Su, *CrystEngComm*, 2013, **15**, 8214; (d) X. Zhang, L. Fan, W. Song, W. Fan, L. Sun and X. Zhao, *RSC Adv.*, 2014, **4**, 30274; (e) L. Fan, W. Fan, B. Li, X. Zhao and X. Zhang, *RSC Adv.*, 2015, **5**, 39854.

12. (a) Y. W. Li, D. C. Li, J. Xu, H. G. Hao, S. N. Wang, J. M. Dou, T. L. Hu and X. H. Bu, *Dalton Trans.,* 2014, **43**, 15708; (b) L. Zhang, J. Guo, Q. Meng, R. Wang and D. Sun, *CrystEngComm*, 2013, **15**, 9578; (c) L. Fan, W. Fan, B. Li, X. Liu, X. Zhao and X. Zhang, *RSC Adv.*, 2015, **5**, 14897; (d) L. L. Liu, C. X. Yu, Y. R. Li, J. J. Han, F. J. Ma and L. F. Ma, *CrystEngComm*, 2015 ,**17**, 653.

13. (a) X. T. Zhang, L. M. Fan, X. Zhao, D. Sun, D. C. Li and J. M. Dou, *CrystEngComm*, 2012, **14**, 2053; (b) L. Fan, Y. Gao, G. Liu, W. Fan, W. Song, L. Sun, X. Zhao and X. Zhang, *CrystEngComm*, 2014, **16**, 7649; (c) L. Fan, X. Zhang, W. Zhang, Y. Ding, W. Fan, L. Sun, Y. Pang and X. Zhao, *Dalton Trans.,* 2014, **43**, 6701; (d) L. Fan, W. Fan, W. Song, L. Sun, X. Zhao and X. Zhang, *Dalton Trans.,* 2014, **43**, 15979.

14. (a) G. Mehlana, S. A. Bourne, G. Ramon and L. Ohrstrom, *Cryst. Growth Des.*, 2013, **13**, 633; (b) L. Fan, X. Zhang, W. Zhang, Y. Ding, L. Sun, W. Fan and X. Zhao, *CrystEngComm*, 2014, **16**, 2144; (c) X. T. Zhang, L. M. Fan, Z. Sun, W. Zhang, D. C. Li, J. M. Dou and L. Han, *Cryst. Growth Des*., 2013, **13**, 792; (d) L. Fan, X. Zhang, Z. Sun, W. Zhang, Y. Ding, W. Fan, L. Sun, X. Zhao and H. Lei, *Cryst. Growth Des.*, 2013, **13**, 2462.

15. (a) G. M. Sheldrick, *SHELXTL*, version 5.1; Bruker Analytical X-ray Instruments Inc.: Madison, WI, 1998. (b) G. M. Sheldrick, *SHELX-97*, PC Version; University of Gottingen: Gottingen, Germany, 1997; (c) SMART, Saint and SADABS; Bruker AXS Inc.: Madison, Wisconsin, USA, 1998.

16. (a) V. A. Blatov, A. P. Shevchenko and V. N. Serezhkin, *J. Appl. Crystallogr.*, 2000, **33**, 1193; (b) V. A. Blatov, M. O'Keeffe and D. M. Proserpio, *CrystEngComm*, 2010, **12**, 44.

17. (a) F. L. Hu, W. Wu, P. Liang, Y. Q. Gu, L. G. Zhu, H. Wei and J. P. Lang, *Cryst. Growth Des*., 2013, **13**, 5058; (b) Q. Q. Li, Y. F. Kang, C. Y. Ren, G. P. Yang, Q. Liu, P. Liu and Y. Y. Wang, *CrystEngComm*, 2015, **17**, 775; (c) M. L. Han, Y. P. Duan, D. S. Li, H. B. Wang, J. Zhao and Y. Y. Wang, *Dalton Trans.,* 2014, **43**, 15450; (d) T. Cao, Y. Peng, T. Liu, S. Wang, J. Dou, Y. Li, C. Zhou, D. Li and J. Bai, *CrystEngComm*, 2014, **16**, 10658.

18. (a) J. Hao, B. Yu, K.V. Hecke and G. Cui, *CrystEngComm*, 2015, **17**, 2279; (b) M. Li, L. Liu, L. Zhang, X. Lv, J. Ding, H. Hou and Y. Fan, *CrystEngComm*, 2014, **16**, 6408; (c) D. -X. Li, C. -Y. Ni, M. -M. Chen, M. Dai, W. -H. Zhang, W. -Y. Yan, H. -X. Qi, Z. -G. Ren and J. -P. Lang, *CrystEngComm*, 2014, **16**, 2158; (d) C. -N. Lü, M. -M. Chen, W. -H. Zhang, D. -X. Li, M. Dai and J. -P. Lang, *CrystEngComm*, 2015, **17**, 1935.

19. (a) L. L. Liu, C. X. Yu, F. J. Ma, Y. R. Li, J. J. Han, L. Lin and J. F. Ma, *Dalton Trans.*, 2015, **44**, 1636; (b) P. Du, Y. Yang, J. Yang, B. K. Liu and J. F. Ma, *Dalton Trans.*, 2013, **42**, 1567; (c) D. X. Li, C. Y. Ni, M. M. Chen, M. Dai, W. H. Zhang, W. Y. Yan, H. X. Qi, Z. G. Ren and J. P. Lang, *CrystEngComm*, 2014, **16**, 2158; (d) L. Zhou, C. Wang, X. Zheng, Z. Tian, L. Wen, H. Qu and D. Li, *Dalton Trans.*, 2013, **42**, 16375.

20. (a) M. Dai, H. -X. Li and J. -P. Lang, *CrystEngComm*, 2015, **17**, 4741; (b) J. Hao, B. Yu, K. V. Hecke and G. Cui, *CrystEngComm*, 2015, **17**, 2279; (c) Y. F. Peng, S. Zhao, K. Li, L. Liu, B. L. Li and B. Wu, *CrystEngComm*, 2015, **17**, 2544; (d) L. Liu, J. Ding, M. Li, Xi. Lv, J. Wu, H. Hou and Y. Fan, *Dalton Trans.*, 2014, **43**, 12790; (e) W. Y. Yin, Z. L. Huang, X. Y. Tang, J. Wang, H. J. Cheng, Y. S. Ma, R. X. Yuan and D. Liu, *New J. Chem.*, 2015, **39**, 7130.

CrystEngComm

For Table of Contents Use Only

Table of Contents Graphic and Synopsis

Coligand Syntheses, Crystal Structures, Luminscence and Photocatalystic Properties of Five Coordination Polymers Based on Rigid Tetracarboxylic Acids and Imidazole Linkers

Liming Fan (L. Fan), Weiliu Fan (W. Fan), Bin Li (B. Li), Xian Zhao (X. Zhao) and Xiutang Zhang (X. Zhang)

Five coordination polymers, featuring various 2D sheets or 3D nets, have been assembled from two rectangular tetracarboxylic acids and imidazole linkers.